and diving through by $\exp(\tau)$ we obtain the standard equation of 1D radiative transfer,

$$\boxed{I(\tau) = e^{-\tau}\left[I(0) + \int_0^{\tau} S e^{\tau'} d\tau'\right]}. \tag{172}$$

We see from the above equation that the optical depth corresponds to an e-folding of the absorption. In other words, in the absence of emission, radiation passing through gas will be attenuated by a factor of e, after one optical depth.

If we can take the gas properties to be constant over the length of interest, S is a constant which can be removed from the integral above. Then eq. (172) becomes:

$$I(\tau) = I(0)e^{-\tau} + S\left(1 - e^{-\tau}\right) \tag{173}$$

$$= S + e^{-\tau}\left[I(0) - S\right] \ . \tag{174}$$

From the above, we can clearly see the asymptotic trends that for an optically-thick medium, with $\tau \to \infty$, we have the intensity approaching the appropriately-named source function, $I \to S$. Similarly, for an optically-thin medium, with $\tau \to 0$, the intensity remains unchanged from the incoming background radiation, $I \to I(0)$.

4.2. The Intergalactic Medium

Thus far in our study of baryons, we have focused on those residing inside dark matter halos, i.e. galaxies. One can argue that they have the most interesting fates. However, the fraction of baryons which reside in galaxies is actually very small: atomic cooling halos host at most a few percent of the baryons at $z \gtrsim 6$. The vast majority of matter lies in the diffuse web stretching between the galaxies, the so-called intergalactic medium (IGM).

The IGM can be characterized by the following fundamental properties: (i) density; (ii) ionization state; (iii) temperature. We discuss each of these in the following sections.

4.2.1. Ionization evolution: the Epoch of Reionization (EoR)

The Epoch of Reionization (EoR) is the last major phase change of the IGM. Light from the first stars and galaxies, discussed in the previous section, spread out throughout the Universe, ionizing and heating the IGM. It is a complex process, encoding the physics of the first structures and how they impacted their surroundings. It is challenging also to model, as the epoch involves a huge range of scales, with the small-scale physics of star formation driving ionization structures which are inhomogeneous on cosmological scales. Here we will establish a basic analytic framework, and encourage readers to delve deeper in the field with reviews such as Mesinger (2016).

Let's begin with an early, star-forming galaxy surrounded by the neutral IGM. Ionizing radiation from its stars can escape the galaxy into the IGM, driving a local, expanding HII region[19] with comoving volume, $V_{\rm HII}$. The evolution of this HII region can be written as:

$$\langle n_{\rm H}\rangle \frac{dV_{\rm HII}}{dt} = \frac{dN_\gamma}{dt} - \alpha_{\rm AB}\langle n_{\rm H}^2\rangle V_{\rm HII} a^{-3} \ . \tag{175}$$

[19]Note that the width of the ionization fronts roughly correspond to the mean free path of the typical ionizing photons. For any UV source, this mean free path in the IGM is very small, of order $\sim$ kpc. Therefore the EoR is an inhomogeneous process with almost fully ionized HII regions around the first galaxies expanding into almost fully neutral HI regions. Here we assume a completely bimodal IGM: either fully neutral or fully ionized. Therefore, we have no ionized fraction terms in eq. (175). In §4.2.3, we shall relax this assumption, which primarily impacts the recombination rate inside the cosmic HII regions.

Here the LHS is the rate at which new HI is ionized as the HII region expands. The first term on the RHS corresponds to the rate (per H atom) at which ionizing photons are escaping the galaxy into the IGM, while the second term corresponds to the average number of recombinations per H atom inside the HII region (note the final a^{-3} term converts the recombination coefficient, $\alpha_{\rm AB}$, [20] to comoving units). For the cosmic HII region to grow, the emission rate of ionizing photons has to be larger than the recombination rate.

We can expand the emission term as a product of the following:

$$N_\gamma = f_{\rm esc} N_{\gamma/b} f_* N_b^{\rm halo} \tag{176}$$

Here the number of baryons in the galaxy is $N_b^{\rm halo}$, f_* is the fraction of those baryons inside stars (c.f. §4.1.5), $N_{\gamma/b}$ is the number of ionizing photons produced per stellar baryon, and $f_{\rm esc}$ the fraction of these ionizing photons which manage to escape into the IGM.

For the absorption term, it is convenient to define a *clumping factor*, $C \equiv \langle n_{\rm H}^2 \rangle / \langle n_{\rm H} \rangle^2$. The clumping factor is a measure of substructure, and should *only be computed inside the ionized regions* which contribute to recombinations. With these definitions, we can rewrite eq. (175) as:

$$\frac{dV_{\rm HII}}{dt} = \frac{1}{\langle n_{\rm H} \rangle} \frac{d[f_{\rm esc} N_{\gamma/b} f_* N_b^{\rm halo}]}{dt} - \alpha_{\rm AB} \langle n_{\rm H} \rangle C V_{\rm HII} a^{-3} \ . \tag{177}$$

To simplify this further, we can assume that the growth of the galaxy, i.e. the $N_b^{\rm halo}$ term, evolves much more rapidly that the other factors in the first term on the RHS. Then if we divide by some "total" (large enough to be representative) volume $V_{\rm tot}$, we obtain the evolution of the filling factor (fraction of total volume) of this particular cosmic HII region:

$$V_{\rm tot}^{-1} \frac{dV_{\rm HII}}{dt} = \frac{f_{\rm esc} N_{\gamma/b} f_*}{V_{\rm tot} \langle n_{\rm H} \rangle} \frac{dN_b^{\rm halo}}{dt} - \alpha_{\rm AB} \langle n_{\rm H} \rangle C \frac{V_{\rm HII}}{V_{\rm tot}} a^{-3} \ . \tag{178}$$

So far we discussed a single HII region. The Universe during the EoR contains many HII regions. We are now in the position to perform an ensemble average over various individual $V_{\rm HII}$. The total ionized volume, summing over all cosmic HII regions is $\sum_i V_{\rm HII}^i$. Analogously, the filling factor of HII regions is $Q_{\rm HII} \equiv V_{\rm tot}^{-1} \sum_i V_{\rm HII}^i$. Finally, we note that $[V_{\rm tot} n_{\rm H}]^{-1} \sum_i N_b^{\rm halo,i} = [N_{\rm tot}]^{-1} \sum_i N_b^{\rm halo,i}$ is the fraction of baryons inside star-forming galaxies. If we assume that star-forming galaxies are hosted by halos with masses above some critical threshold mass (set by cooling or feedback), $M_{\rm min}$, then the fraction of baryons

[20] The recombination coefficient for a given species (hydrogen or helium) is usually written as being either "case A", $\alpha_{\rm A}$, or "case B", $\alpha_{\rm B}$. The case A coefficient includes the sum of probabilities of a recombination to *any* state (including directly to the ground state), while the case B excludes recombinations directly to the ground state (which result in the emission of an ionizing photon). For hydrogen at a temperature of 10^4 K, we have $\alpha_{\rm A} = 4.2 \times 10^{-13}$ cm^3 s^{-1}, and $\alpha_{\rm B} = 2.6 \times 10^{-13}$ cm^3 s^{-1} (e.g. Osterbrock 1989). When computing the ionization balance of the IGM, it is more appropriate to use case A if the recombinations are taking place in optically-thick systems (at low redshifts referred to as Lyman limit systems; LSSs). The reasoning behind this is that the photons resulting from ground state recombinations are likely to be absorbed locally, inside the LLS). After some number of ionizations/absorptions, the recombination happens into an excited state, and there is no more ionizing photon. Thus the ionizing photons resulting from ground state recombinations do not escape the LLS, and so do not contribute to the ionization balance in the diffuse IGM (Miralda-Escudé 2003). The case B recombination coefficient is more appropriate when recombinations are happening in more diffuse, optically thin systems. In this case, the ground state photon can travel in the IGM, and result in another IGM ionization. As a result this photon is ionization neutral when computing the IGM ionization state, and so is not counted in the rate equations. While it is clear that for the post-reionization IGM the case A is more appropriate, it is really not clear what is better at high redshifts, as it depends on knowing the properties of the systems which are dominating the recombinations (are they occurring mostly in dense systems or in the actual diffuse IGM which one is modeling). In the next chapter, we develop the framework for studying recombining systems, but current uncertainties in the strength of the ionizing background prevent us from knowing which recombination coefficient is more appropriate. In this chapter therefore, we use a general notation, $\alpha_{\rm AB}$, to indicate that the appropriate coefficient is somewhere between case A and case B.

inside star-forming galaxies is just the collapsed fraction, $f_{\rm coll}(> M_{\rm min})$ from §3.3. With this ensemble averaging, we arrive at the evolution of the HII filling factor:

$$\boxed{\frac{dQ_{\rm HII}}{dt} = f_{\rm esc} N_{\gamma/b} f_* \frac{df_{coll}(> M_{\rm min}, z)}{dt} - \alpha_{\rm AB} \langle n_{\rm H} \rangle C a^{-3} Q_{\rm HI}} \; . \tag{179}$$

Each of the parameters in the above equation is the subject of topical research.

- *The fraction of galactic baryons inside stars, f_*,* depends on the efficiency of star formation, as discussed in §4.1.5. Simple estimates which scale the halo mass function by a constant amount to fit the LF suggest values of order $f_* \sim$ per cent, for the bulk of the high-redshift galaxy population (e.g. Vale & Ostriker 2006; Dijkstra et al. 2014; Dayal et al. 2014, Park et al. in prep).

- *The typical number of ionizing photons produced per stellar baryon, $N_{\gamma/b}$,* depends on the IMF of the stars. Population II stars should produce roughly 5000 ionizing photons over their lifetime, while more top-heavy IMFs or metal-free PopIII stars could increase this number by an order of magnitude (see e.g. Fig. 13 and Tumlinson & Shull 2000; Schaerer 2002).

- *The halo mass threshold for star-formation, $M_{\rm min}$,* depends on cooling efficiency or feedback, and can take on values ranging between $M_{\rm min} \sim 10^6 M_\odot$ for the first, molecularly-cooled halos (e.g. Bromm et al. 2002; Abel et al. 2002; Yoshida et al. 2008), $M_{\rm min} \sim 10^8 M_\odot$ for atomically-cooled halos. If feedback was efficient in quenching star formation in these small-mass halos the threshold could be as high as $M_{\rm min} \sim 10^{10} M_\odot$, corresponding the faintest high-redshift galaxies observed today (see Fig. 16).

- *The fraction of ionizing photons which escape the galaxy, $f_{\rm esc}$,* depends on the galactic morphologies and the corresponding distribution of column densities. These in turn are likely set by a combination of dynamical and thermal evolution, with strong SNe feedback episodes likely clearing away the surrounding medium, facilitating the escape of ionizing photons. Direct observations of Lyman continuum emission are impossible at high redshifts given current technology. Stacks of Lyman break galaxies at lower redshifts, $z \sim 3$–4, motivate typical values of $f_{\rm esc} \sim$ per cent (e.g. Steidel et al. 2001; Shapley et al. 2006; Siana et al. 2007; Marchi et al. 2017); however fainter galaxies at high redshifts are expected to have higher escape fractions as low column density sightlines are easier to be created by SNe explosions in shallower potential wells (e.g. Paardekooper et al. 2015; Xu et al. 2016). If $M_{\rm min}$ is much larger the atomic cooling threshold, so that only rare bright galaxies drive the EoR, we would need to have escape fractions of order tens of per cent to have the Universe reionize by $z \sim 5$–6 (e.g. Mitra et al. 2013; Kuhlen & Faucher-Giguere 2012; Robertson et al. 2013; Greig & Mesinger 2017).

- *The clumping factor inside the ionized IGM, C,* is expected to be of order unity – few for the bulk of reionization, but could be much larger in the initial EoR stages if the ionized gas is heated and smoothed as its Jeans mass increases (e.g. Emberson et al. 2013; Pawlik et al. 2017), or rise rapidly in the later stages of the EoR as the ionization fronts penetrate into increasingly dense clumps thus allowing higher densities to contribute to the recombination rate (e.g. Furlanetto & Oh 2005; Sobacchi & Mesinger 2014; see §4.2.3).

We can simplify eq. (179) even further if we assume that these astrophysical parameters are redshift-independent. In this case, we can integrate over cosmic time:

$$Q_{\rm HII}(z) = f_{\rm esc} N_{\gamma/b} f_* \int_\infty^{z(t)} \frac{df_{\rm coll}(> M_{\rm min}, z)}{dt'} dt' - \int_\infty^{z(t)} \frac{dn_{\rm rec}}{dt'} dt' \tag{180}$$

$$= f_{\rm esc} N_{\gamma/b} f_* f_{\rm coll}(> M_{\rm min}, z) - n_{\rm rec}(z) \; , \tag{181}$$

where the number of recombinations per baryon is explicitly denoted as $n_{\rm rec}$. To first order, we can take the recombinations to be linearly distributed in $Q_{\rm HII}$ (i.e. assuming a weaker dependence on the other terms). This allows us to write:

$$Q_{\rm HII}(z) \approx f_{\rm esc} N_{\gamma/b} f_* f_{\rm coll}(> M_{\rm min}, z) - \bar{n}_{\rm rec} Q_{\rm HII}(z) \ , \tag{182}$$

where $\bar{n}_{\rm rec}$ is the total number of recombinations per baryon during the EoR. Finally, we have:

$$\boxed{Q_{\rm HII}(z) \approx \frac{f_{\rm esc} N_{\gamma/b} f_*}{(1+\bar{n}_{\rm rec})} f_{\rm coll}(> M_{\rm min}, z)} \tag{183}$$

As seen from eq. (183), the EoR only depends on the product of the aforementioned astrophysical quantities. Therefore, it is common to define this product as an "ionizing efficiency", ζ:

$$\zeta \equiv 20 \left(\frac{f_{\rm esc}}{0.1}\right) \left(\frac{f_*}{0.03}\right) \left(\frac{N_{\gamma/b}}{5000}\right) \left(\frac{1.5}{1+\bar{n}_{\rm rec}}\right) \tag{184}$$

with eq. (183) becoming simply:

$$\boxed{Q_{\rm HII} = \zeta f_{\rm coll}} \ . \tag{185}$$

Patchy Reionization

Finally, it is important to remember that reionization by UV photons is a very inhomogeneous process, with a fraction $\sim Q_{\rm HII}$ of the Universe virtually fully ionized, while the remaining $1-Q_{\rm HII}$ is virtually fully neutral. The topology of this process thus tells us how the star-forming galaxies are spatially distributed. We can simulate this patchy reionization with large radiative transfer simulations; however the results are uncertain as we do not know the ionizing efficiencies of galaxies. Luckily, we can build some intuition analytically. As was noted by Furlanetto et al. (2004), we can use the same excursion-set tools we used to build the halo mass functions.

We can rephrase the global evolution in eq. (185), by realizing that each sub-region of the Universe is itself ionized if:

$$\zeta f_{\rm coll}(> M_{\rm min}, z | M_{\rm HII}, \delta_{\rm HII}) \geq 1 \ . \tag{186}$$

Here we have replaced the global collapsed fraction, with the conditional one: the fraction of matter inside collapsed structures above $M_{\rm min}$ at z, *given* that they reside in a large-scale region that has a matter overdensity $\delta_{\rm HII}$ on a scale $M_{\rm HII}$. We can express this conditional collapsed fraction as (§3.3):

$$f_{\rm coll}(> M_{\rm min}, z | M_{\rm HII}, \delta_{\rm HII}) = {\rm erfc}\left[\frac{\delta_{\rm crit}(z) - \delta_{\rm HII}}{\sqrt{2[\sigma^2(M_{\rm min}) - \sigma^2(M_{\rm HII})]}}\right] \ . \tag{187}$$

Plugging this into eq. (186), and inverting the complimentary error function:

$$\frac{\delta_{\rm crit}(z) - \delta_{\rm HII}}{\sqrt{2[\sigma^2(M_{\rm min}) - \sigma^2(M_{\rm HII})]}} \leq {\rm erfc}^{-1}(\zeta^{-1}) \ . \tag{188}$$

Therefore, we can stipulate that a region of scale $M_{\rm HII}$ is ionized at redshift z, if it has an overdensity of:

$$\boxed{\delta_{\rm HII} \geq \delta_{\rm crit}(z) - {\rm erfc}^{-1}(\zeta^{-1})\sqrt{2[\sigma^2(M_{\rm min}) - \sigma^2(M_{\rm HII})]}} \tag{189}$$

This overdensity is analogous to the "critical overdensity" for the collapse of dark matter halos. In §3.3, we constructed a halo mass function from the distribution of first upcrossings of the barrier $\delta_{\rm crit}$. Analogously, here we can construct the "HII region mass function" from the distribution of first upcrossings of the barrier $\delta_{\rm HII}$. This can be done either numerically, or analytically by linearizing the function in σ^2: $\delta_{\rm HII} \equiv B_0 + B_1\sigma^2(M)$. The constants B_0 and B_1 can be obtained by considering the asymptotic limit on large-scales, $\sigma^2(M_{\rm HII}) \to 0$. In this large-scale limit, the barier becomes $\delta_{\rm HII} \to B_0 =$

$\delta_{\rm crit} - {\rm erfc}^{-1}(\zeta^{-1})\sqrt{2[\sigma^2(M_{\rm min}) - \cancelto{0}{\sigma^2(M_{\rm HII})}]} = \delta_{\rm crit} - \sqrt{2}\sigma(M_{\rm min}){\rm erfc}^{-1}(\zeta^{-1})$. Moreover the slope of the barrier becomes $\partial\delta_{\rm HII}/\partial\sigma^2 \rightarrow B_1 = {\rm erfc}^{-1}(\zeta^{-1})/\sqrt{2[\sigma^2(M_{\rm min}) - \cancelto{0}{\sigma^2(M_{\rm HII})}]} = {\rm erfc}^{-1}(\zeta^{-1})/\sqrt{2\sigma^2(M_{\rm min})}$. Having a linear barrier allows us to use the ellipsoidal functional form derivation of the halo mass function by Sheth et al. (2001). In analogy to the linear ellipsoidal barrier used for the ST mass functions, we can write the HII bubble mass fuction, i.e. the comoving number density of HII regions of mass scale $M_{\rm HII} \sim (4/3)\pi R_{\rm HII}^3\bar{\rho}$, as (Furlanetto et al. 2004):

$$\boxed{\frac{dn}{d\ln M_{\rm HII}} = \sqrt{\frac{2}{\pi}}\frac{\bar{\rho}}{M_{\rm HII}}\left|\frac{d\ln\sigma}{d\ln M_{\rm HII}}\right|\frac{B_0}{\sigma}\exp\left[\frac{(B_0 + B_1\sigma^2)^2}{2\sigma^2}\right]} \tag{190}$$

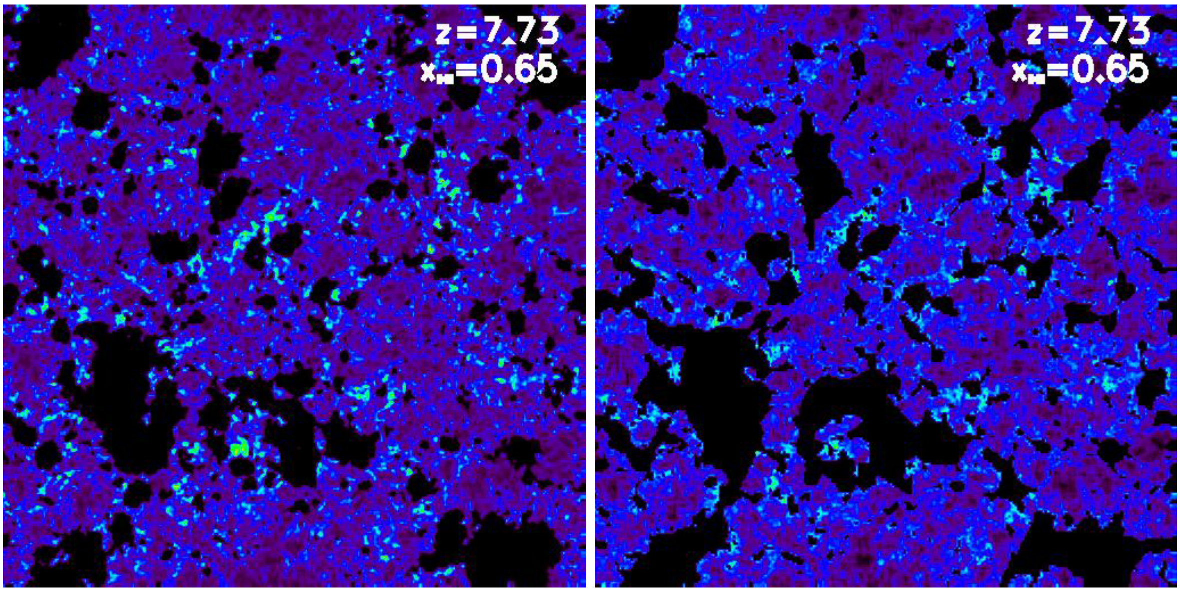

Fig. 18.— Slices through a simulated 21-cm signal during the EoR, with black corresponding to cosmic ionized patches (from Mesinger et al. 2011). The left panel was generated from a hydrodynamic radiative-transfer simulation, while the right panel was generated using an analytic excursion-set procedure applied to density fields which were evolved with the ZA. Both share the same initial conditions. All slices are 143 Mpc on a side and 0.56 Mpc thick.

In addition to the analytic "HII mass function", the excursion-set approach discussed above has been applied directly to 3D realizations. This is computationally very efficient, since smoothing the 3D density field to obtain $f_{\rm coll}(> M_{\rm min}, z|M_{\rm HII}, \delta_{\rm HII})$ just involves doing an FFT on the scale $M_{\rm HII}$. Starting from some maximum scale corresponding to a horizon for ionizing photons, the criterion from eq. (186) is evaluated at each cell of the simulation. Cells which reside in sufficiently large overdensities smoothed on that scale are marked as ionized. Then the smoothing scale is decreased and the procedure is iterated.

Ionization fields obtained with this procedure are in a good agreement with computationally-intensive radiative transfer methods, on moderate to large scales ($\gtrsim$ 1 Mpc; e.g. Zahn et al. 2011; see also Fig. 18). The conditional collapsed fraction from eq. (186) can be computed using (i) the halo field directly from N-body simulations (Zahn et al. 2007); (ii) the halo field from perturbation theory (Mesinger & Furlanetto 2007); (iii) the evolved density field (Mesinger et al. 2011). The later, although a little more approximate, has the advantage of facilitating a nearly unlimited dynamical range. This is important when modeling the signal on very large scales, such as is required for 21-cm observations (see §4.3).

4.2.2. *Current EoR probes*

Our current knowledge about the EoR stems from two classes of probes: (i) integral constraints from the CMB in the form of the Thompson scattering optical depth to the lass scattering surface (LSS)[21]; and (ii) astrophysical "flashlights" which illuminate the intervening IGM. We briefly discuss each in turn.

Optical depth to the CMB

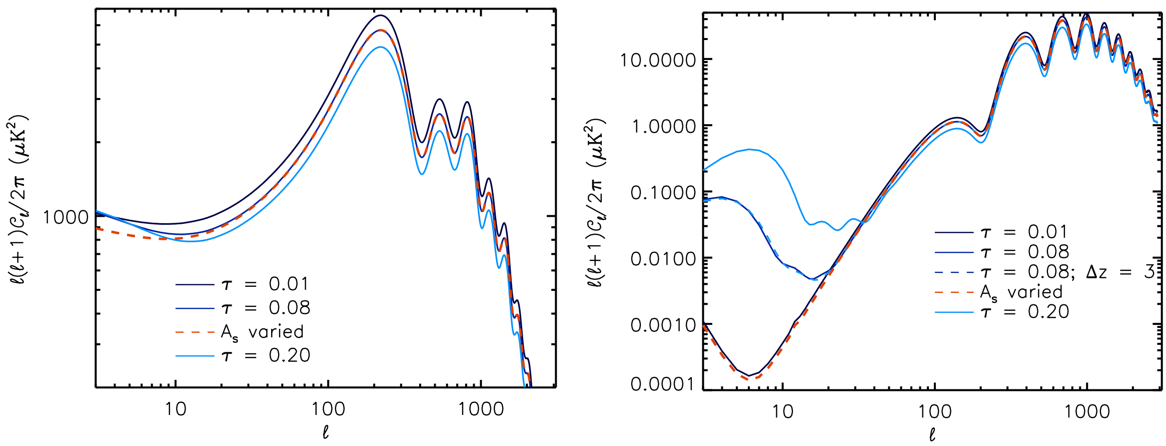

Fig. 19.— CMB temperature (*left*) and E-mode (zero curl) polarization (*right*) power spectra, for several different values of the mean Thompson scattering optical depth, τ_e. Increasing τ_e dampens the temperature fluctuations; however, this effect is strongly degenerate with reducing the primordial amplitude, A_s. Although a far weaker signal, the large-scale polarization fluctuations do not suffer from this degeneracy. These figures are taken from Reichardt (2016).

As light from the last scattering surface (LSS; i.e. the CMB) passes through the Universe, it interacts with free electrons through Thompson scattering. Thompson scattering is gray scattering, thus the dominant effect is to dampen the CMB temperature fluctuations, as light from hot spots gets scatter into lines of sight towards cold spots, and visa versa. The more free electrons (corresponding to an earlier EoR), the stronger is the distortion of the primordial CMB.

This imprint of the EoR can be characterized through the mean Thompson scattering optical depth,

$$\tau_e = \langle \int_0^{z_{\rm LSS}} n_e \sigma_T \left| \frac{cdt}{dz} \right| dz \rangle_{\rm LOS} \tag{191}$$

Here, n_e is the electron number density, σ_T the Thompson scattering cross-section, $c\ dt$ the line element to the LSS, and the averaging is performed over all lines of sight (LOSs). Thus the higher the τ_e, the more the CMB temperature fluctuations are damped (see the left panel of Fig. 19). This damping is easy to detect. Unfortunately, it is also strongly degenerate with the primordial power spectrum amplitude, A_s, as shown in the left panel of Fig. 19.

Luckily, the CMB has a large-scale quadrupole anisotropy. This means the EoR creates a linear polarization signal in the CMB, which peaks on scales larger than the horizon during the EoR. Unlike for the temperature power spectra, the impact of τ_e on the polarization power spectra is *not* degenerate with cosmology (see the right panel of Fig. 19). Unfortunately, this signal is much weaker and more difficult to detect, compared to the temperature fluctuations.

[21] Alternative probes such as E-mode polarization as a function of angular scale (e.g. Mortonson & Hu 2008), the patchiness of τ_e (e.g. Dvorkin & Smith 2009), the kinetic Sunyaev-Zel'dovich signal from patchy reionization (e.g. Mesinger et al. 2012), could yield interesting results in the future provided systematics can be controlled (see the review of Reichardt 2016).

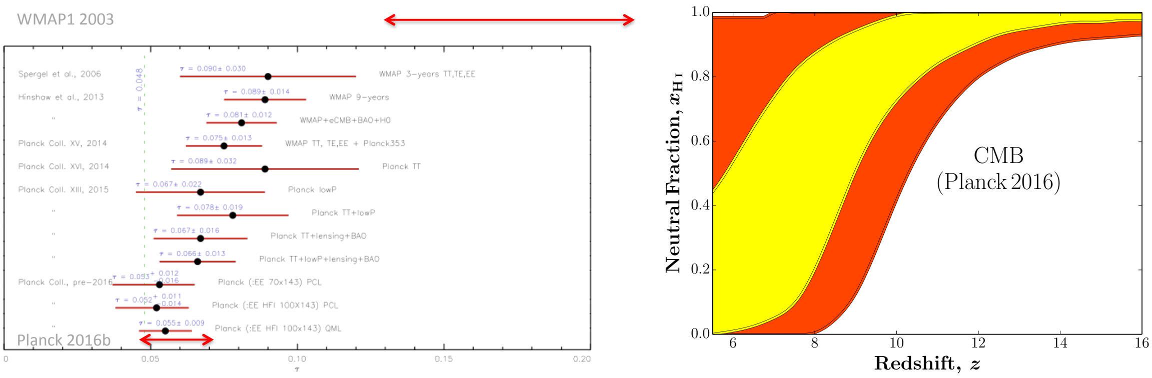

Fig. 20.— *Left*: Historical trend of the 1 σ constraint on the mean Thompson scattering optical depth to the CMB, τ_e. Figure is adapted from Planck Collaboration XLVI et al. (2016), with the addition of the 1-yr *WMAP* result of $\tau_e = 0.17 \pm 0.04$ using only the temperature power spectrum at the top (Kogut et al. 2003) and the alternate HFI estimate from Planck Collaboration XLVII et al. (2016) $\tau_e = 0.058 \pm 0.012$ at the bottom. *Right*: Constraints on the evolution of the average neutral fraction, $\bar{x}_{\rm HI} = 1 - Q_{\rm HII}$, corresponding to the latest *Planck* estimate of $\tau_e = 0.058 \pm 0.12$ (Planck Collaboration XLVII et al. 2016). 68% C.L. are shown in yellow, while 95% C.L. are shown in red. $\bar{x}_{\rm HI}(z)$ was sampled from physically-motivated EoR models, based on eq. (183), with the optical depth used to compute a χ^2 likelihood. Taken from Greig & Mesinger (2017).

In the left panel of Fig. 20, we show the historical trend of τ_e estimates. Starting with the *WMAP* satellite, the first estimate using only the temperature power-spectra was $\tau_e = 0.17 \pm 0.04$ (1σ) (Kogut et al. 2003). This unexpectedly-high optical depth implied there were *abundant* ionizing sources in the very Universe ($z > 15$), at a time when the furthest objects were at $z \sim 6$. The resulting implications on structure formation caused much excitement/confusion in the community.

However, in subsequent years the value of τ_e decreased, with the errors shrinking. This was driven mainly by the addition of polarization data, first through the temperature-polarization cross-power spectra and then through the detection of the polarization auto power spectra with the *Planck* satellite. The current (2017) conservative estimate is $\tau_e = 0.058 \pm 0.012$ (Planck Collaboration XLVII et al. 2016), obtained using *Planck*'s high frequency instrument (HFI).

How does this constrain the reionization history? Because τ_e is an integral measurement, it cannot tell us about the duration and patchiness of the EoR. Translating τ_e to a reionization history requires assuming a functional form for $Q_{\rm HII}(z)$. In the right panel of Fig. 20 we show the 1-σ (*yellow*) and 2-σ (*red*) constraints on the reionization history created by sampling EoR models based on eq. (183), using $\tau_e = 0.058 \pm 0.012$ to compute a χ^2 likelihood, and marginalizing over the free parameters in the model. We see that the mean reionization redshift implied by Planck Collaboration XLVII et al. (2016) is $z = 7.64^{+1.34}_{-1.82}$. We caution however that the exact shape of these EoR history constraints are model-dependent, depending on the $Q_{\rm HII}(z)$ functionals and their corresponding priors.

Lyα damping wing absorption

The Lyα line of hydrogen has emerged as a powerful probe of the EoR. To understand its utility, let's consider the schematic shown in Fig. 21. Sources during the EoR (galaxies and QSOs) emit an intrisic Lyα flux (*bottom right panel*), whose profile is set by local and interstellar properties of the source. These photons emerge from the galaxy/QSO into some local patch of the IGM, which has already been ionized by the contribution from neighboring sources; the residual HI inside these local ionized patches (*top right panel*) is determined by the local density and ionizing radiation, as we shall see in the next section. The photons pass through the local HII region, redshifting along the way. Those which are not scattered out of the line of sight by the residual HI inside the local ionized patch then pass through the large-scale EoR topology of cosmic HI and HII regions (*left panel*), redshifting as they travel towards us.

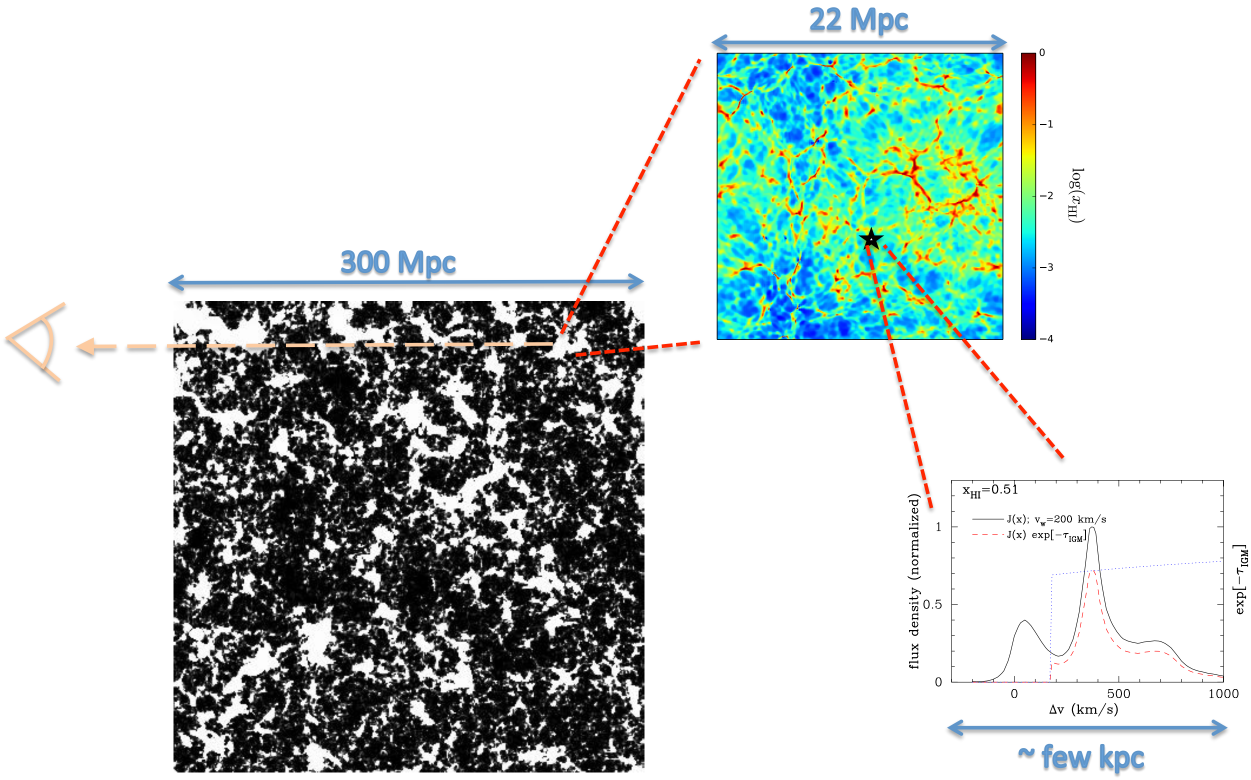

Fig. 21.— Schematic showing the various components determing the observed Lyα line from high redshift QSOs and galaxies druring the EoR. From left to right we show: (i) a 0.75 Mpc thick slice through large-scale reionization simulation at $Q_{\rm HII} \sim 0.5$ (Sobacchi & Mesinger 2014); (ii) a 21 kpc slice through hydro simulation of the ionized IGM surrounding high-z galaxies (Mesinger et al. 2015); (iii) the intrinsic Lyα line emerging from a galaxy including RT through local outflows (Dijkstra et al. 2011).

The observed flux at a wavelength, $\lambda_{\rm obs}$, for a source at redshift $z_{\rm s}$ can be expressed as:

$$F_{\rm obs}(\lambda_{\rm obs}) = F_0 \left(\frac{\lambda_{\rm obs}}{1+z} \right) e^{-\tau(\lambda_{\rm obs})} , \tag{192}$$

where F_0 is the intrinsic (i.e. emerging from the galaxy/QSO into the IGM) spectrum, evaluated at a rest frame wavelength $\lambda_{\rm obs}/(1+z)$, and the total IGM optical depth due to Lyα absorption, τ, is given by (neglecting peculiar velocities):

$$\tau(\lambda_{\rm obs}) = \int_0^{z_{\rm s}} dz \, \frac{c\, dt}{dz} \, n_H \, x_{\rm HI} \, \sigma \tag{193}$$

where $c(dt/dz)$ is the proper line element in a given cosmology, $n_H(z)$ is the hydrogen number density at redshift z, $x_H(z)$ is the hydrogen neutral fraction at redshift z, and $\sigma[\lambda_{\rm obs}/(1+z)]$ is the Lyα absorption cross section.

As described above, each source sits inside a local HII region, allowing the total optical depth to be separated into a component sourced by the resonant absorption, τ_R, and that from the damping wing of the cross section, τ_D. The common practice is to use the size of the local HII region, R_S, to separate the terms:

$$\begin{aligned} \tau &= \tau_R + \tau_D \\ &= \int_{z_{\rm HII}}^{z_{\rm s}} d\tau_R + \int_{z_{\rm end}}^{z_{\rm HII}} d\tau_D \, . \end{aligned} \tag{194}$$

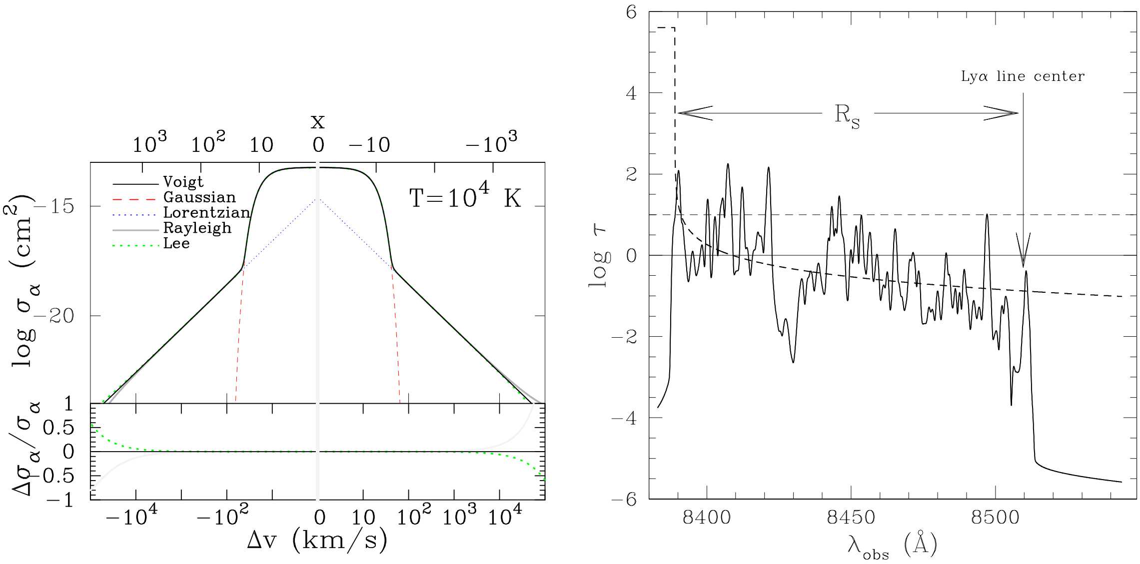

Fig. 22.— *Left:* Lyα cross section. Like all line transitions, the Lyα cross section consists of a relatively narrow core, whose width is set by a combination of turbulent motions and thermal Doppler broadening, and Lorenzian tails extending far from the core of the line (e.g. Rybicki & Lightman 1979). The figure is taken from Dijkstra (2014). *Right:* Optical depth contributions from within (τ_R) and from outside (τ_D) the local HII region for a typical line of sight towards a $z_s = 6$ quasar embedded in a fully neutral IGM. The *dashed line* corresponds to τ_D, and the *solid line* corresponds to τ_R. In this example, the damping wing of the IGM, τ_D, contributes significantly to the total optical depth at $\lambda_{\rm obs} \sim 8430$ Å and $\lambda_{\rm obs} \gtrsim 8470$ Å. The figure is taken from Mesinger & Haiman (2007).

Here $z_{\rm HII}$ corresponds to the redshift of the edge of the local HII region, and z_{end} denotes the redshift by which HI absorption is insignificant along the line of sight to the source (of order a hundred Mpc from the source).

The two components in eq. (194) are qualitatively different, as can be seen from the right panel of Fig. 22. Due to the relatively narrow core, τ_R pics up density and residual HI fluctuations inside the local HII region; thus it is a rapidly fluctuating quantity resulting in the so-called Lyα forest in QSO spectra. On the other hand, the damping wing is a smooth function of wavelength, averaging over opacity fluctuations over relatively large scales.

The strength of the damping wing absorption depends directly on the neutral fraction of the IGM. Studies looking for the imprint of the damping wing in galaxy and QSO spectra either focus on its spectral smoothness (e.g. Mesinger & Haiman 2004, 2007; Schroeder et al. 2013) or on the absolute absorption on the red side of the Lyα line where resonant absorption is negligible (e.g. Miralda-Escude 1998; Haiman & Spaans 1999; Santos et al. 2004; Bolton et al. 2011; Mesinger et al. 2015). In fact the later approach was used by Greig et al. (2017) to obtain the first detection (2σ) of ongoing reionization from the spectrum of a bright $z = 7.1$ quasar (see Fig. 23).

Combining current probes

Fig. 24 summarizes the current state of knowledge on the history of reionization (pre-2017; taken from Greig & Mesinger (2017); see also similar results by Mitra et al. (2015); Price et al. (2016)). Fitting a physically-motivated basis set of $\bar{x}_{\rm HI}(z)$ to current observations, these authors constrain the epochs corresponding to an average neutral fraction of (75, 50, 25) per cent, to $z = (8.52^{+0.96}_{-0.87}, 7.57^{+0.78}_{-0.73}, 6.82^{+0.78}_{-0.71})$, (1-$\sigma$). The strongest constraints here come from the *first detection of ongoing reionization*, obtained from the spectra of the $z = 7.1$ QSOs ULASJ1120+0641: $\bar{x}_{\rm HI}(z = 7.1) = 0.4^{+0.41}_{-0.32}$ (2-σ); see also the recent work by Mason et al. (2017) who obtain comparable limits from the disappearance of Lyman alpha emitting galaxies beyond $z \gtrsim 6$ (not shown in the figure).

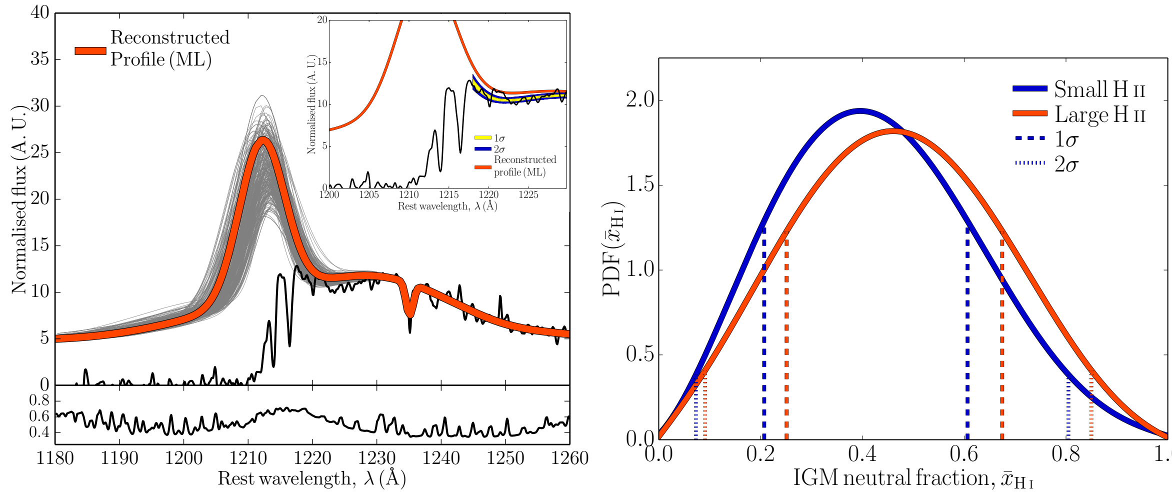

Fig. 23.— *Left:* FIRE spectrum of the $z = 7.08$ QSO, ULASJ1120+0641 is shown in black (Simcoe et al. 2012). The intrisic emission, F_0, of the QSO (before it passes through the intervening IGM) is shown in red (maximum likelihood) and gray (sampling the posterior), obtained by using the reconstruction procedure of Greig et al. (2017). The zoom-in inset also shows the 1 and 2 σ uncertainty on the total observed spectrum, $F_0 e^{-\tau_D}$, with τ_D computed from the simulations of Mesinger et al. (2016). The fact that the total observed spectrum is systematically higher than the intrinsic one is evidence of a non-zero τ_D from ongoing reionization. *Right:* The PDFs of $\bar{x}_{\rm HI} = 1 - Q_{\rm HII}$, quantifying the imprint of the damping wing shown in the right panel. The two curves correspond to opposite extreme assumptions about the topology of the EoR. *Figures are taken from Greig et al. (2017).*

4.2.3. Density evolution

Neglecting the impact of radiation, the density distribution of the IGM can be obtained by evolving the continuity equations from §4.1.1. The linear evolution of gas was already discussed above, when discussing the initial stages of collapse. However the IGM is only quasi-linear; thus hydrodynamic simulations are also used to obtain its density field. Fig. 25 shows the gas distribution from such a simulation by Viel et al. (2010) (*top left panel*), together with the corresponding DM field (*bottom left panel*). On large scales, the gas and dark matter trace each other very well, while on small scales the baryons are more diffuse owing to pressure support (note that the Jeans length in the mean density, ionized IGM is $\sim 0.6\sqrt{(1+z)/10}$ cMpc). On sub-galactic scales this trend is reversed, as radiative cooling allows baryons to collapse to much higher densities, creating stars and black holes.

For many applications, it would be very useful to have an analytic or parametric model of the IGM density distribution. In the linear regime, the density PDF is a Gaussian centered on $\Delta \equiv \rho/\bar{\rho} = 1$. We would expect structure formation to result in an extended tail towards large Δ, thus shifting the median of the distribution to $\Delta < 1$ (i.e. the under dense, so-called "voids" take up most of the volume of the Universe). This behavior is evident in Fig. 26. We could also expect the width of the distribution to be related to the Jeans scale. Using these guiding principles, Miralda-Escudé et al. (2000) (hereafter MHR00) proposed the following parametric form for the volume-weighted density PDF:

$$P(\Delta, z) = A\Delta^{-\beta} \exp\left[-\frac{(\Delta^{-2/3} - C_0)^2}{2(2\delta_0/3)^2}\right] . \tag{195}$$

where A and C_0 are constants set by volume and mass normalization, at each redshift:

$$\int_0^\infty P(\Delta) d\Delta = 1 \; ; \tag{196}$$

$$\int_0^\infty \Delta P(\Delta) d\Delta = 1 \; . \tag{197}$$

In the limit of $\delta_0 \ll 1$ and $C_0 \rightarrow 1$, we would recover the linear density field behavior, with the distribution approaching a Gaussian in $\Delta - 1$, with a dispersion of δ_0. Thus we expect $\delta_0 \propto (1+z)^{-1}$ following the

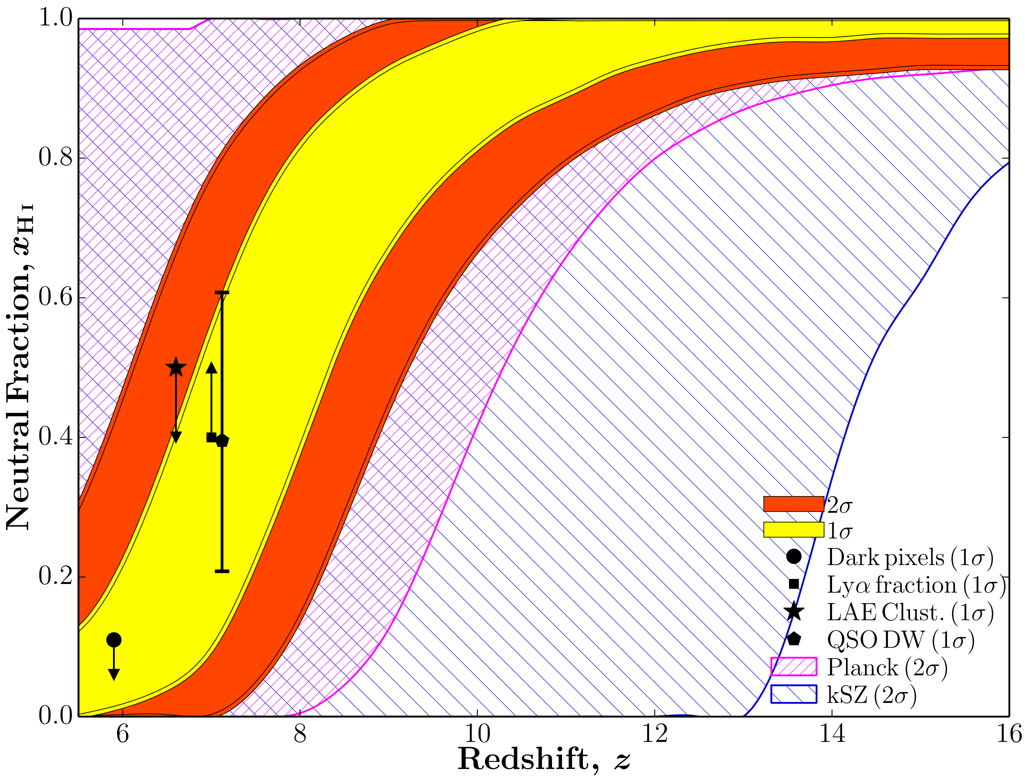

Fig. 24.— Constraints on the evolution of the average neutral fraction, $\bar{x}_{\rm HI} = 1 - Q_{\rm HII}$, from various probes (pre-2017). A physically-motivated EoR model was sampled, with the likelihood of each resulting $\bar{x}_{\rm HI}(z)$ curve provided by current observations. The figure is taken from Greig & Mesinger (2017).

evolution of the linear Growth factor in matter-dominated cosmologies. MHR00 take $\delta_0 \propto 7.61(1+z)^{-1}$, with the proportionality constant fit to match hydrodynamic simulations. The final constant, $\beta(z) \sim 2.2$–2.5, is also fit to simulation outputs at $z = 2$–4, though again we can "guesstimate" its value by noting that in the $\Delta \gg 1$ tail of the distribution which probes collapsed structures, the exponential factor in eq. (195) approaches unity. Thus the total distribution approaches $P(\Delta) \propto \Delta^{-\beta}$. If we assume collapsed structures, i.e. halos, follow an isothermal density profile: $\Delta(r) \propto r^{-2}$, then the fraction of the halo volume with density greater than $> \Delta$ is $V(> \Delta) \propto r^3 \propto \Delta^{-3/2}$, making the volume-averaged probability density scale as $P(\Delta) = dV(> \Delta)/d\Delta \propto \Delta^{-5/2}$. Thus isothermal structures result in $\beta = 2.5$, close to the fit found by MHR00.

How well does eq. (195) reproduce simulations? This can be seen from Fig. 27. Although there are some physically-motivated trends in eq. (195), *it is still an empirical fit to simulations* and therefore the agreement in the left panel (the original work from MHR00) is understandable. Bolton & Becker (2009) subsequently revisited this functional form and tested its agreement against larger simulations, over a more extended redshift range out to $z = 6$. Their results are shown in the right panel of Fig. 27. They find that the MHR00 form is accurate to withing a few percent over two decades around $\Delta = 1$, becoming increasingly inaccurate for large values. Note however that the high value tail is not known even in simulations, since the density distribution of gas in and around galaxies is very sensitive to SNe feedback (e.g. McQuinn et al. 2011).

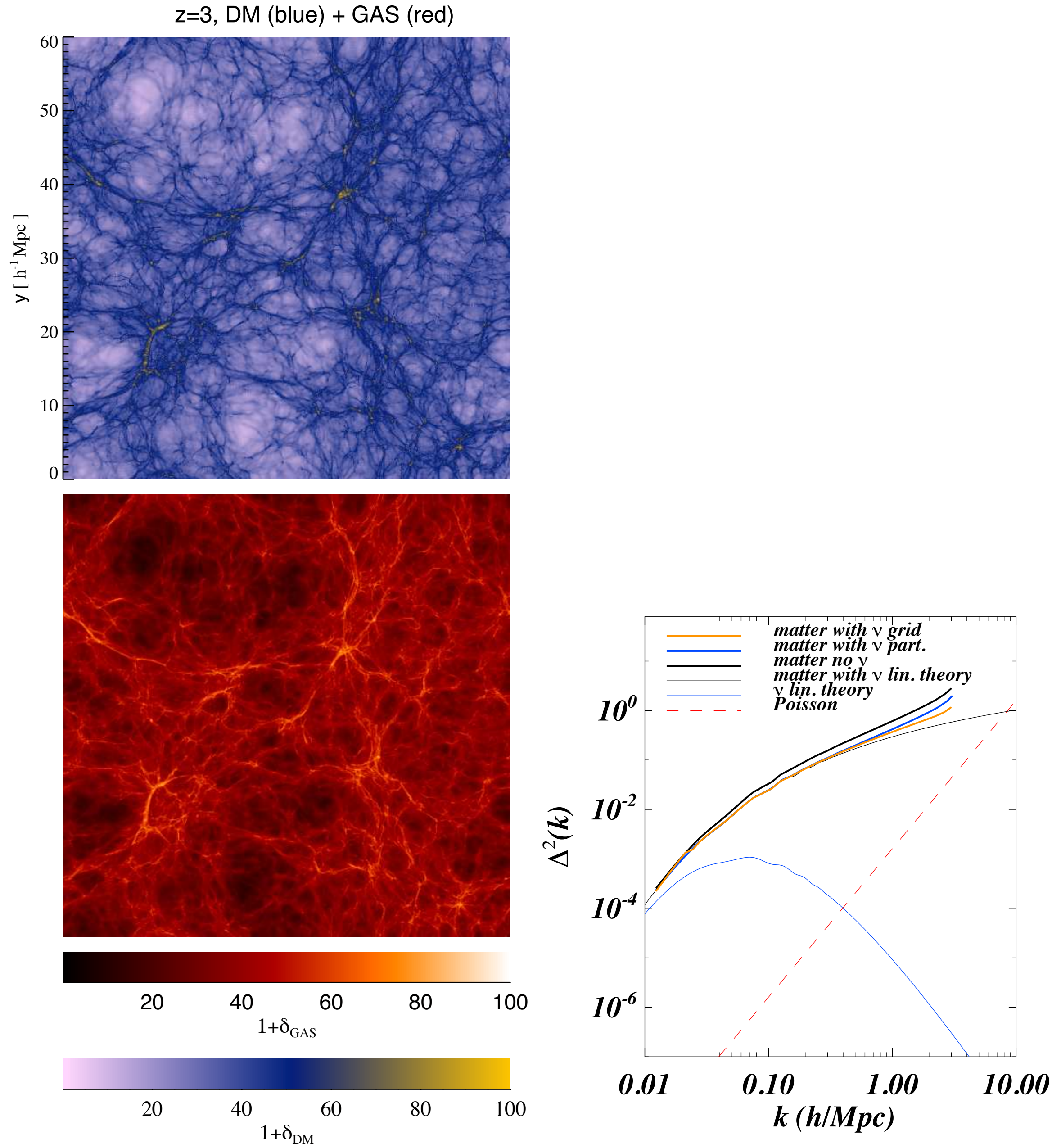

Fig. 25.— The simulated intergalactic medium at $z = 3$. The top left shows a 6 h^{-1} Mpc slice through the dark matter distribution in a 512^3 simulation, while the panel below it shows the correspond baryon field. Note that on large scales, the gas and dark matter trace each other very well, while on small scales the baryons are more diffuse owing to pressure support. On sub-galactic scales this trend is reversed, as radiative cooling allows baryons to collapse to much higher densities, creating stars and black holes. On the right, there is the corresponding dimensionless power spectra, including some models with massive neutrinos. Neutrino free streaming results in a suppression of small scale structure. The figures are taken from Viel et al. (2010).

Corresponding HI structure

As we saw in the previous section, observables generally do not depend only on the IGM density, but on the combination of the density and neutral fraction. In the (ionized) Universe, we can expect low density regions to be optically thin to ionizing radiation, while dense clumps are optically thick, capable of self-shielding against the ionizing background radiation. MHR00 also proposed a bi-modal model for self-shielding, shown in Fig. 28, with a critical density threshold separating the optically thin regime from the optically thick regime.

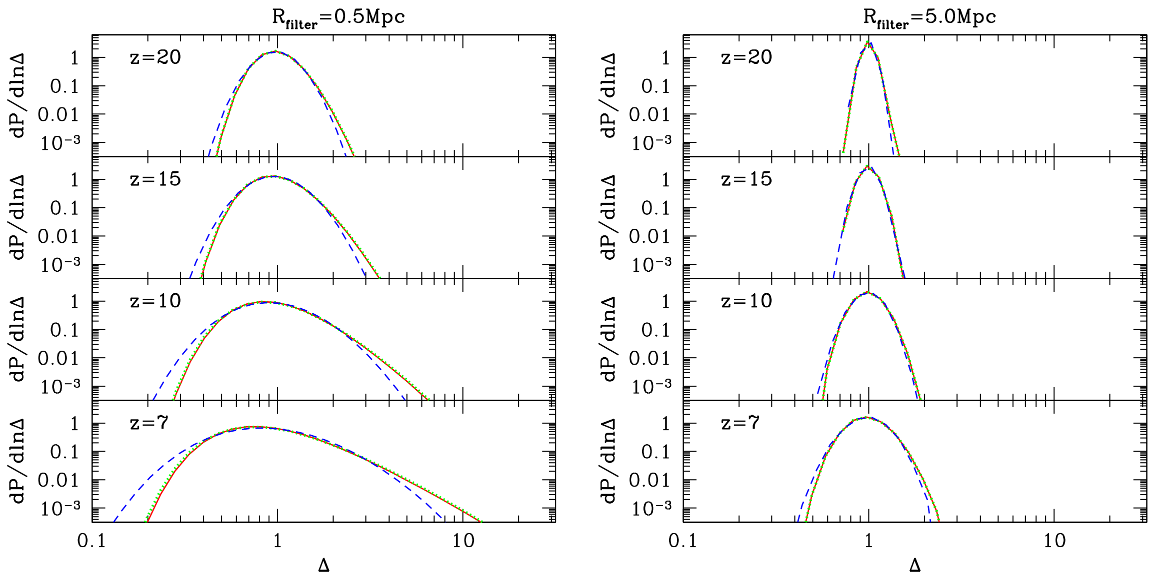

Fig. 26.— Volume-averaged PDFs of the density fields ($\Delta \equiv \rho/\bar{\rho}$) smoothed on scale $R_{\rm filter}$, computed from a 143 Mpc on a side, 1024^3 simulation of the gas (*solid red curves*), DM (*dotted green curves*), and linear perturbation theory (ZA; *dashed blue curves*) fields, at z = 20, 15, 10, 7 (top to bottom). The left panel corresponds to $R_{\rm filter}$ = 0.5 Mpc; the right panel corresponds to $R_{\rm filter}$ = 5 Mpc. At early times and large scales, the density field is still fairly linear (approaching a Gaussian in $\Delta - 1$, with a dispersion of σ_M). Non-linearity as one approaches late times and small scales is evident in the appearance of the high value tail, with the median of the distribution shifting to under-densities (matching the visual trends seen in the previous figure. All smoothing was performed with a real-space, top-hat filter. The figures are taken from Mesinger et al. (2011).

In this model, the gas sees a local ionizing background, $\Gamma(\Delta)$, which instantaneously transitions from the impinging (usually taken to be the mean) ionizing background, $\Gamma_{\rm bg}$, to zero at the critical self-shielding density:

$$\Gamma(\Delta) = \begin{cases} \Gamma_{\rm bg} & \text{if } \Delta < \Delta_{\rm ss} \\ 0 & \text{if } \Delta > \Delta_{\rm ss} \end{cases} \tag{198}$$

The above step function is a reasonable approximation, resulting in recombination rates similar to what is seen in simulations (see below) but over-estimating the neutral hydrogen content of $\Delta \gg \Delta_{\rm ss}$ systems (e.g. McQuinn et al. 2011; Rahmati et al. 2013; Keating et al. 2014; Mesinger et al. 2015). The transition from optically thin to optically thick is more gradual, and depends somewhat on the spectral shape of the ionizing background (harder photons can penetrate deeper into clumps). Using a Haardt & Madau (2001) UV background, Rahmati et al. (2013) provide an empirical fit to their hydrodynamic simulations which show a more gradual self-shielding, in better agreement with observations of HI column densities:

$$\Gamma(\Delta) = \Gamma_{\rm bg} \times \left\{ 0.98 \left[1 + \left(\frac{\Delta}{\Delta_{\rm ss}} \right)^{1.64} \right]^{-2.28} + 0.02 \left[1 + \frac{\Delta}{\Delta_{\rm ss}} \right]^{-0.84} \right\} \tag{199}$$

Can we compute the characteristic self-shielding overdensity $\Delta_{\rm ss}$*?* Let's begin by first discritizing the density field into self-gravitating clouds on the *local* (i.e. Δ-dependent) Jeans scale, i.e. the distance a pressure wave can travel in a free-fall time (Schaye 2001):[22]

$$L_{\rm J} \equiv \frac{c_s}{\sqrt{G\rho}} \ . \tag{200}$$

[22]Note that the 1D distance is a more robust quantity than the Jeans mass, which assumes a 3D geometry for the conversion from scale to mass.

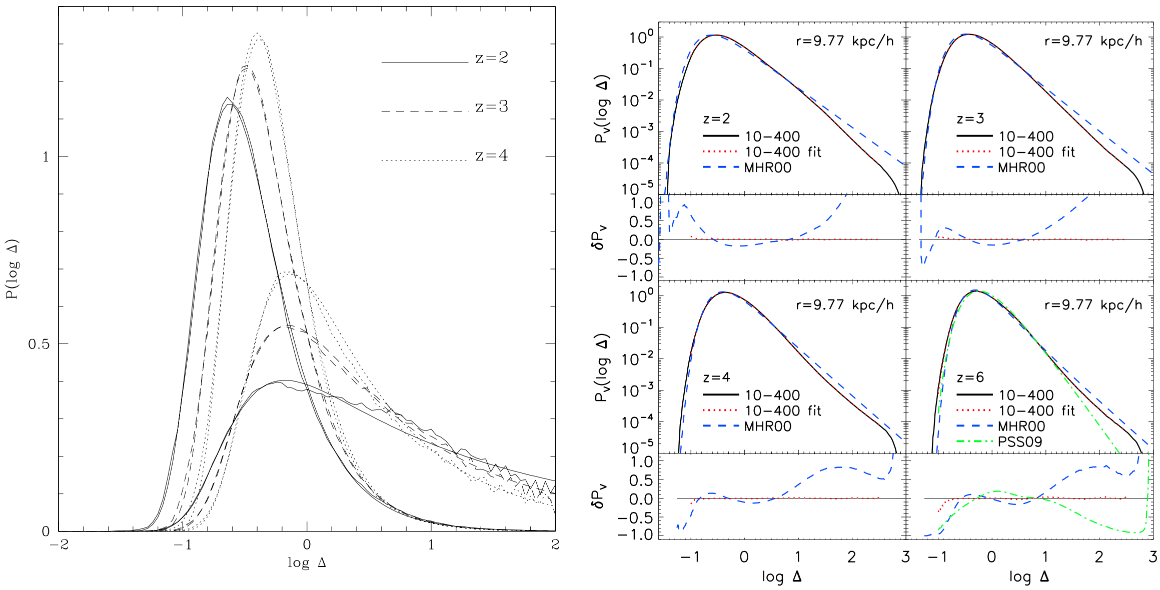

Fig. 27.— Density PDFs. On the left, we have the original results from Miralda-Escudé et al. (2000); the lines with noise correspond to a hydrodynamic simulation while the smooth curves correspond to their analytic fit. Narrow distributions are volume weighted, i.e. $P(\Delta, z)$, while broad distributions are mass weighted, i.e. $\Delta P(\Delta, z)$. On the right we have an analogous study by Bolton & Becker (2009) showing how the MHR00 distribution, although accurate at the percent level for two decades around the mean, becomes inaccurate at high densities for this model. It is worth noting that the true density distribution in the high value tail is sensitive to SNe feedback, and is poorly understood.

Taking $c_s^2 = \frac{\gamma k_B T}{\mu m_p}$ and $\rho = \left(\frac{1}{f_g}\right) \rho_{\rm gas} = \left[\frac{1}{f_g(1-Y_{\rm He})}\right] \rho_{\rm H}$, where f_g is the fraction of the total mass in gas, $f_g(1-Y_{\rm He})$ is the fraction of the total mass in hydrogen, and $\rho_{\rm H} = m_p n_{\rm H}$ is the mass density of hydrogen, we can write:

$$\begin{aligned} L_{\rm J} &= \sqrt{\frac{\gamma k_B T}{\mu m_p}} \sqrt{\frac{f_g(1-Y_{\rm He})}{G m_p n_{\rm H}}} \\ &= \sqrt{\frac{\gamma k_B}{G m_p^2}} \sqrt{\frac{f_g}{\mu}} \sqrt{\frac{T}{\Delta \bar{n}_{\rm H}}} \ . \end{aligned} \tag{201}$$

The first factor is just made of constants, while the second factor can change somewhat due to ionization ($\mu = 0.6/1.2$ for an ionized/neutral medium, and we expect the gas fraction to be close to the cosmic mean value Ω_b/Ω_m). The final factor can vary significantly. For reference, the typical Jeans length inside galaxies can be $\sim$ pc, while the typical Jeans length inside the (ionized) IGM can be $\sim$ Mpc at high redshifts.

Given the Jeans length of our gas element, we can compute the corresponding HI column density, $N_{\rm HI}$, to see if it is sufficient to self-sheild:

$$\begin{aligned} N_{\rm HI} &= x_{\rm HI} \Delta \bar{n}_{\rm H} L_{\rm J} = x_{\rm HI} \sqrt{T \Delta} \sqrt{\frac{\gamma k_B f_g \bar{n}_H}{G \mu m_p^2}} \\ &= 1.5 \times 10^{20} {\rm cm}^{-2} \ x_{\rm HI} \sqrt{T_4 \Delta_{100}} Z_7^{3/2} \ , \end{aligned} \tag{202}$$

where we take $\gamma = 5/3$ for a monatomic gas, $f_g = \Omega_b/\Omega_m \approx 0.17$, $\mu = 0.6$, and subscripts in the last line denote the values used for normalization: $T_4 \equiv T/10^4$K, $\Delta_{100} \equiv \Delta/100$, $Z_7 \equiv (1+z)/7$. The corresponding optical depth is obtained by multiplying with the ionization cross section, $\sigma_{\rm LL} \sim 6 \times 10^{-18}$ cm^2, resulting in: $\tau = N_{\rm HI} \sigma_{\rm LL} \approx 10^3 x_{\rm HI} \sqrt{T_4 \Delta_{100}} Z_7^{3/2}$. *Thus, even gas with a modest fraction of neutral hydrogen (our default values correspond to* $x_{\rm HI} > 10^{-3}$*), can self-shield against ionizing radiation.*

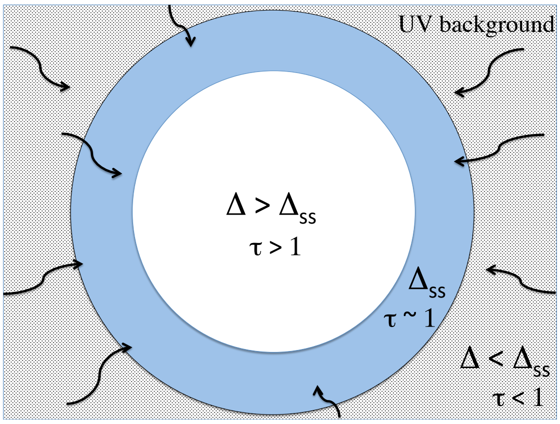

Fig. 28.— Simple model for the ionization structure of gas illuminated by a pervasive ionizing background. Roughly spherical, self-gravitating clumps have a thin shell with overdensity, $\Delta_{\rm ss}$, corresponding to an optical depth of unity. Gas inside this shell is self-shielded from the ionizing background, and remains largely neutral.

Since highly ionized gas can self shield, in computing $\Delta_{\rm ss}$ we can simplify the equation of ionization equilibrium, i.e.

$$x_{\rm HI} n_{\rm H} \Gamma = (1 + f_{\rm He}) \left[n_{\rm H}(1 - x_{\rm HI})\right]^2 \alpha_{\rm A} \ , \tag{203}$$

to its $x_{\rm HI} \ll 1$ limit:

$$x_{\rm HI} = \frac{(1 + f_{\rm He}) n_{\rm H} \alpha_{\rm A}}{\Gamma} \ , \tag{204}$$

where $f_{\rm He} = (4/Y_{\rm He} - 3)^{-1} \approx 0.077$ is the helium number fraction, and we assume helium is singly-ionized together with hydrogen (an accurate assumption given their comparable energy thresholds). Taking the empirical fit for the recomination coefficient from Cen (1992): $\alpha_{\rm A}(T) \approx 4.2 \times 10^{-13}\ T_4^{-0.7}$ cm^3 s^{-1}, and defining $\Gamma_{12} = \Gamma/(10^{-12}{\rm s}^{-1})$, we have:

$$x_{\rm HI} \approx 3 \times 10^{-3}\ \Gamma_{12}^{-1} T_4^{-0.7} \Delta_{100} Z_7^3 \ . \tag{205}$$

Putting this into eq. (202) we have:

$$N_{\rm HI, x_{HI} \ll 1} \approx 4.5 \times 10^{17} {\rm cm}^{-2}\ \Gamma_{12} T_4^{-0.2} \Delta_{100}^{3/2} Z_7^{9/2} \ . \tag{206}$$

If we define $\Delta_{\rm ss}$ to be the value for which $\tau = N_{\rm HI, x_{HI} \ll 1} \sigma_{\rm LL} = 1$, we obtain:

$$\boxed{\Delta_{\rm ss} \approx 50\ \Gamma_{12}^{2/3} T_4^{0.13} Z_7^{-3}} \tag{207}$$

We now have the framework to calculate one of the fundamental quantities for the IGM: the recombination rate. The recombination rate per hydrogen atom is computed by integrating over the density distribution:

$$\frac{dn_{\rm rec}}{dt} = \int_0^\infty \Delta^2 \bar{n}_{\rm H}\ \alpha_{\rm A}\ \left[1 - x_{\rm HI}\right]^2\ P\ d\Delta \ . \tag{208}$$

Here the density PDF, P, can be computed from eq. (195), and the neutral fraction, $x_{\rm HI}$, from eq. (203). In Fig. 29 we show the evolution of the mean emissivity (*thick curves*) and recombination rate (*thin curves*) for several simulations in which the above framework was included via a sub-grid prescription (taken from Sobacchi & Mesinger 2014). The most complete model is denoted as "FULL". Towards the end stages of reionzation ($\bar{x}_{\rm HI} \lesssim 0.1$), the recombination rate balances the emission rate of ionizing photons (see also Furlanetto & Oh 2005), resulting in a so-called "photon-starved" end to reionization (e.g. Bolton & Haehnelt 2007).

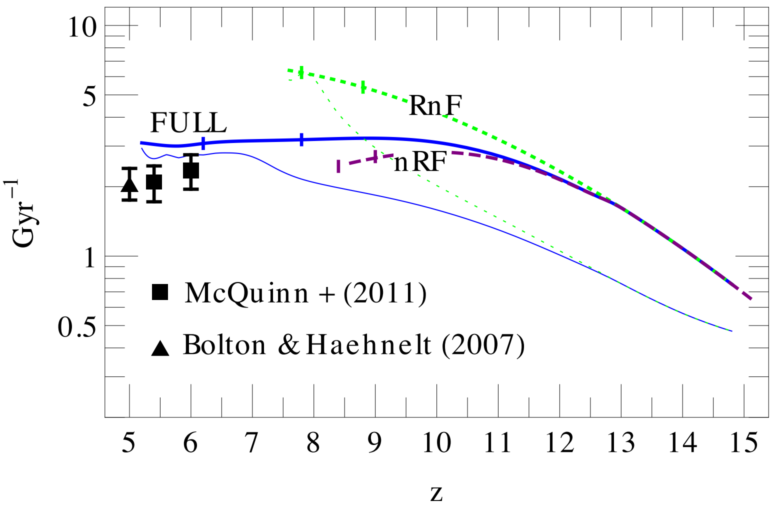

Fig. 29.— Evolution of the average emissivity (*thick*) and recombination rate per baryon (*thin*) with different models in Sobacchi & Mesinger (2014). The most complete model is denoted as "FULL". The vertical ticks correspond to $\bar{x}_{\rm HI} = 0.2$ and $\bar{x}_{\rm HI} = 10^{-2}$. For comparison we show the emissivity constraints inferred from the Ly α forest at $z \lesssim 6$ (Bolton & Haehnelt 2007; McQuinn et al. 2011).

4.2.4. Thermal evolution

Gas in the IGM behaves as a classical ideal gas, which quickly reaches local thermal equilibrium (LTE). In LTE, the temperature of any gas component with number density n_i and internal energy U_i can be written as:

$$\begin{aligned} T &= \frac{2U_{\rm i}}{3k_B n_{\rm i}} \\ &= \frac{2U_{\rm tot}}{3k_B n_{\rm tot}} \end{aligned} \tag{209}$$

The second line follows from equipartition of energy in an ideal gas in LTE. $U_{\rm tot}$ is the total internal energy per unit volume, and $n_{\rm tot}$ is the total number density of the gas, composed primarily of hydrogen and helium:

$$\begin{aligned} n_{\rm tot} = \sum_i n_i &\approx n_e + n_{\rm HI} + n_{\rm HII} + n_{\rm HeI} + n_{\rm HeII} \\ &\approx x_i(n_{\rm H} + n_{\rm He}) + (1 - x_i)n_{\rm H} + x_i n_{\rm H} + (1 - x_i)n_{\rm He} + x_i n_{\rm He} \\ &= x_i(n_{\rm H} + n_{\rm He}) + n_{\rm H} + n_{\rm He} \\ &= n_b(1 + x_i) \end{aligned} \tag{210}$$

As in the previous section, here we assume that hydrogen and helium are singly ionized with an ionization fraction of x_i; thus $n_e = x_i(n_{\rm H} + n_{\rm He})$. Moreover, we ignore doubly-ionized Helium (assuming $n_{\rm HeIII}$=0), whose high ionization threshold requires very hard sources, and is thus expected to be ionized with the advent of QSOs at lower redshifts, $z \lesssim 4$.

We can explicitly solve for the evolution of the IGM temperature of an IGM gas element, starting with the time derivative of eq. (209):

$$\frac{dT}{dt} = \frac{2}{3k_B}\left[\frac{1}{n_{\rm tot}}\frac{dU_{\rm tot}}{dt} - \frac{U_{\rm tot}}{n_{\rm tot}^2}\frac{dn_{\rm tot}}{dt}\right]$$